Conf-9504154--1

UCRL-JC- 119069
PREPRINT

Buried Mine Detection Using Ground-Penetrating Impulse Radar

P.D. Sargis

This paper was prepared for submittal to the

Autonomous Vehicles in Mine Countermeasures Symposium

Monterey, Ca
April 3-7, 1995

March 1995

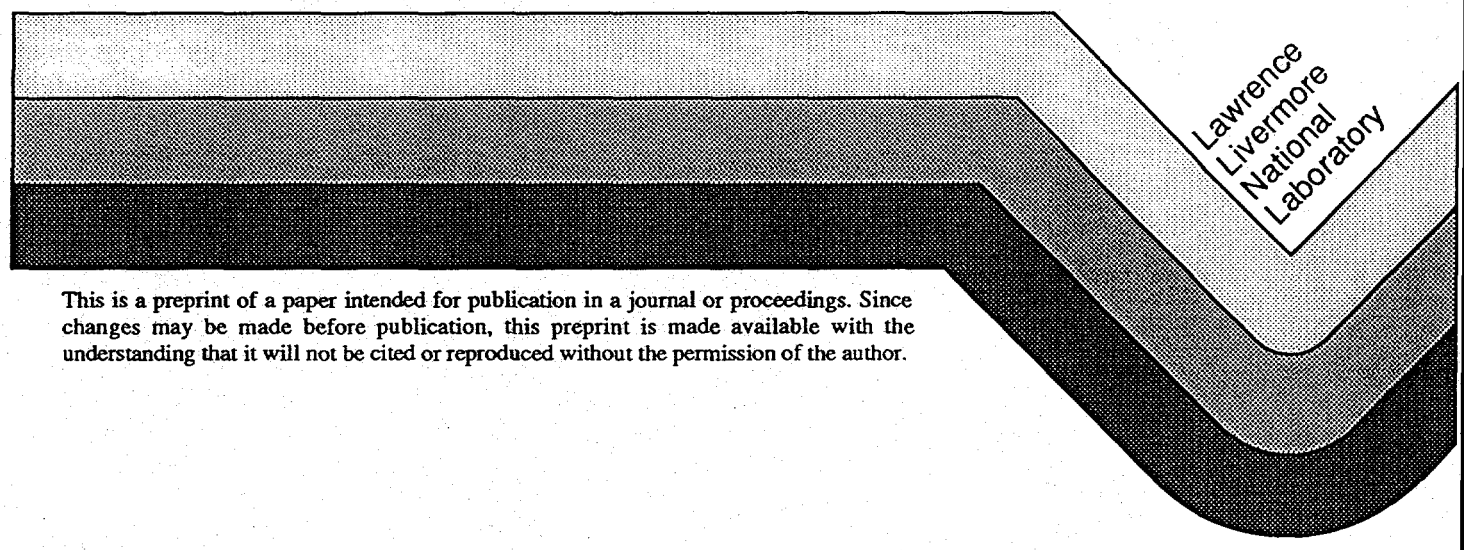

GH

DISCLAIMER

Buried Mine Detection Using Ground-Penetrating Impulse Radar

Paul D. Sargis

Lawrence Livermore National Laboratory (LLNL)
P.O. Box 808, M/S L-54, Livermore, CA 94551

***Abstract*—LLNL is developing a side-looking, ground-penetrating impulse radar system that can eventually be mounted on a robotic vehicle or an airborne platform to locate buried land mines. The system is described and results from field experiments are presented.**

I. INTRODUCTION

Various types of synthetic-aperture radar (SAR) systems can be applied to the problem of locating buried mines and minefields. High-altitude airborne SAR systems have the advantage of being able to search large areas quickly, but they require high-power transmitters to couple adequate energy into the ground. Ground-coupled systems can penetrate deeply into the soil, but they require travel over the surface of the site being surveyed and only provide data over a narrow swath. LLNL's "standoff" ground-penetrating radar (GPR) system is mounted above the roof of a van, simulating a slow-moving, low-flying airborne platform. It can examine areas up to ten meters wide with a penetration depth that is between that of airborne and ground-coupled systems.

Instead of using a pulse-modulated swept-frequency technique, this system uses an impulse approach, because of its relative simplicity and because of LLNL's expertise in impulse generation, transient digital recording, and SAR processing. This approach is based on some of the techniques developed by SRI International.[1,2]

Advanced image reconstruction software was previously developed for other LLNL SAR projects, and was adapted for use on the mine detection project. Both the hardware and software aspects of LLNL's GPR system can be applied to the problem of detecting unexploded ordnance.

II. SYSTEM DESCRIPTION

As shown in Figure 1, the system is currently installed in a self-contained van with the antennas mounted at a fixed elevation of four meters. A simple block diagram of the GPR system is presented in Figure 2. The trigger source for the system is a shaft encoder on a friction wheel against one of the vehicle tires. A trigger pulse is issued whenever the wheel turns a selected fraction of a revolution. When prompted by the shaft encoder, the trigger generator distributes triggers to the pulse transmitter, a pulse counter, and a transient digitizer with appropriate delays to compensate for cable lengths.

The pulse transmitter is a LLNL-designed unit which uses avalanche transistor technology to generate the high-voltage video pulse shown in Figure 3. The spectral content of the transmitter was optimized over the passband of interest using pulse-shaping techniques. (See Figure 4.) Optimum power transfer occurs when the spectral content of the transmitter matches the response of the transmit antenna. If the transmitter generates significant energy outside the passband of the antenna, it will reflect back toward the transmitter. This energy may then reflect a second time from the transmitter output, causing interfering pulses to be transmitted from the antenna.

The transmit antenna, pictured in Figure 5, is a commercial double-ridged horn antenna and is designed to operate from 200 MHz to 2000 MHz. Although the 3-dB antenna beamwidth varies with frequency, it is on the order of 45 degrees in both the E-plane and the H-plane.

The receive antenna, shown in Figure 6, is a unique design. The monopole corner reflector uses a folded triangle element to permit operation from 400 MHz to 1500 MHz. This design has several advantages over a conventional resistive dipole corner reflector. It has considerably more gain than a resistive dipole, it is half the size, and it takes a simple coaxial feed with an autotransformer matching network. Its geometry minimizes crosstalk from the adjacent horn antenna. Like the horn antenna, the 3-dB beamwidth for this antenna varies with frequency. It is on the order of 40 degrees in both the E-plane and the H-plane.

The frequency response of the pair of antennas is plotted in Figure 7. They are capable of efficiently transmitting a pulse having spectral content between 400 MHz and 1500 MHz. Because the monopole corner reflector has a narrower bandwidth than the horn, it is used on the receiver rather than on the transmitter because it rejects local VHF two-way radio signals.

The combined response of the transmitter, antennas, and coaxial cables is well behaved. (See Figure 8.) A frequency-domain representation of this response, shown in Figure 9, reveals that the GPR system performs well between 400 MHz and 1000 MHz. The narrower bandwidth of the monopole corner reflector acts as a filter for the horn antenna to produce this clean response. Experience has shown that the use of identical antennas for transmission and reception yields a response that rings.

A Hewlett-Packard 54720D 4 gigasample per second transient digitizer functions as the receiver. The digitizer's internal amplifier is used to take advantage of its full eight-bit resolution. When triggered, the 54720D captures a 256-point waveform. Each waveform is transferred to an Apple Macintosh IIfx and stored in RAM until the data run is complete. (The data acquisition and instrument control software is written in National Instruments LabVIEW, a high-level object-oriented software package.) Finally, the data is transferred to a Sun or HP workstation for SAR processing.

The antennas are mounted on a remotely-controlled pan-and-tilt mechanism, permitting adjustment of the antenna look angle. The transmitted pulse is optimally refracted into the ground when the antenna tilt angle matches the Brewster angle, as determined by the soil dielectric constant at the center of the spectrum. This is illustrated in Figure 10. Maximum penetration depth varies, depending on the conductivity of the soil.

III. THE NTS MINE DETECTION FACILITY

LLNL operates the Buried Object and Mine Detection Facility at the Nevada Test Site (NTS), which is located in the high desert, approximately 100 km northwest of Las Vegas. This facility appears in the foreground of the photograph in Figure 11. Actual mines (without detonators) and surrogate mines, both metal and plastic, have been buried in natural vegetation. The soil in this area is made up of alluvium, consisting of Paleozoic fragments and tuff. Soil conductivity is on the order of five to eight millisiemens per meter. The exact location of buried mines has been carefully documented. Figure 12 shows how the facility is laid out. An area has been cleared of vegetation and smoothed to permit evaluation of the GPR system with a minimum of ground clutter.

Figure 13 illustrates the typical layout of a minefield plot. Items marked "fid" are 10-cm square galvanized steel plates that are used as surface markers. The fids are attached to the ground by means of short metal skewers. At each end of a minefield, three 1-cm diameter rebars are driven approximately 30 cm into the ground, leaving 60 cm above ground. Mines and surrogates are buried with between one and ten centimeters of soil overburden. The actual location of objects varies from the square grid when bushes are present. Vegetation and burrows were left intact to maintain realistic conditions.

IV. EXPERIMENTAL RESULTS

The GPR system discussed in section 3 was set up at the Nevada Test Site, and the antennas were positioned at an elevation of five meters. Both antennas were mounted for vertical polarization, and the antenna look angle was 34 degrees below horizontal to center the main antenna lobe over the middle row of objects. The angle from the antennas to the back row of objects was around 26 degrees. For an estimated dielectric constant of 4 at the center of the spectrum, the angle to the back row approximates the Brewster angle. Thus, Brewster's law favors the back row of objects, the antenna pattern favors the middle row, and close range favors the front.

Data was collected every five cm along the road adjacent to the minefield designated, "I-south." This minefield contains real metal mines (without detonators) and surrogate mines, all of which are approximately 30 cm in diameter. Figure 14 is a 140x256 composite image of data from subplot IS-4 with the average background subtracted. It is a side-by-side representation of the 140 time-domain data records. The three rows of objects clearly stand out above the clutter. Each object is defined by an arc. Prior to SAR processing, the image is preprocessed using average subtraction, range compensation, and pulse compression. Average subtraction takes the difference between the raw image and the mean of the raw image. Range compensation corrects for power losses due to the distance from the antennas to the objects. Pulse compression deconvolves the antenna-to-antenna system pulse response (Figure 8) from the result to reduce ringing and improve resolution.

Figure 15 is the reconstructed SAR image of minefield I-south, subplot 4. Object positions in this image correspond to arc positions in Figure 14 . With the addition of the exact location of objects in Figure 16, there is good correlation between the ground-truth registration and the GPR result. The three-dimensional representation of this data in Figure 17 shows that most of the clutter is well below the buried objects and surface markers. A visual analysis of the minefield showed that the stronger returns from clutter were due to bushes and animal burrows. Overall, the signal-to-clutter ratio in this image is between 4:1 and 6:1.

V. SUMMARY

LLNL has demonstrated the capability of its standoff, wideband, side-looking GPR system to locate buried metal mines with a signal-to-clutter ratio of up to 6:1 at the Mine Detection Facility at the Nevada Test Site. Reconstructed two-dimensional images of the test area compare favorably with the ground truth data, and validate the capabilities of the system.

ACKNOWLEDGMENT

The support of Dean Lee, Steve Fulkerson, William Aimonetti, David Fields, Michael Carter, Charles Anderson, Terry Rossow, Jeff Mast, and Erik Johansson of LLNL is gratefully acknowledged. The efforts of the field support team from EG&G, North Las Vegas are also appreciated.

REFERENCES

1. D. R. Rutt, "Use of an ultra-wideband synthetic aperture radar technique for buried mine detection," SPIE Vol. 1875, Ultrahigh Resolution Radar 1993, pp. 68-76, 20 January 1993.

2. R. S. Vickers, V. H. Gonzalez, and R. W. Ficklin, "Results from a VHF impulse synthetic aperture radar," SPIE Vol. 1631, Ultrawideband Radar 1992, pp. 219-225, 22-23 January 1992.

Work performed under the auspices of the U.S. Department of Energy by Lawrence Livermore National Laboratory under Contract No. W-7405-Eng-48.

Figure 1. Self-contained GPR Data Acquisition Vehicle

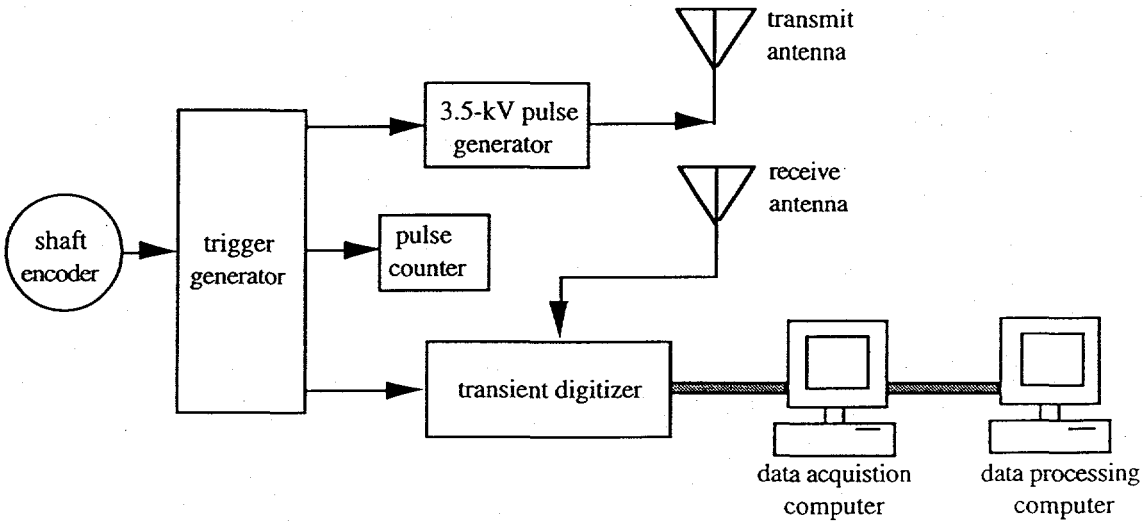

Figure 2. Block Diagram of GPR System

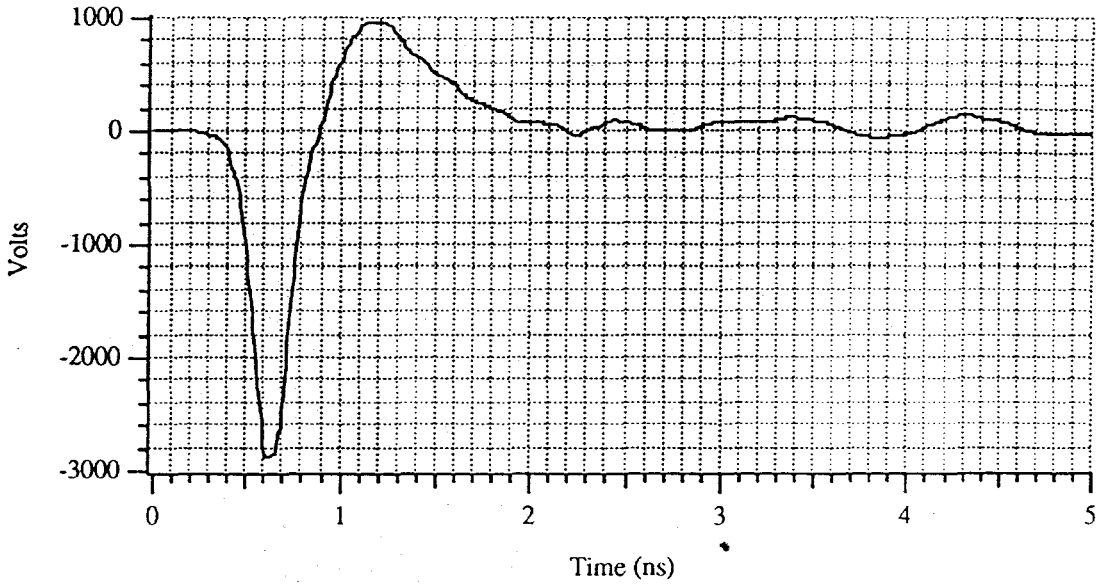

Figure 3. Pulse transmitter output waveform

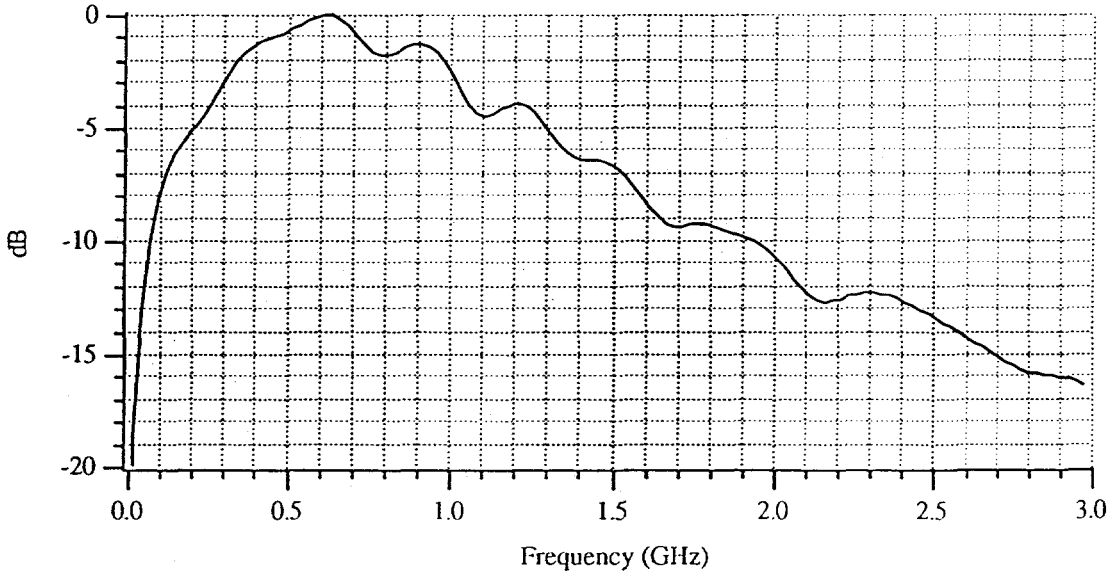

Figure 4. Spectrum of pulse transmitter output

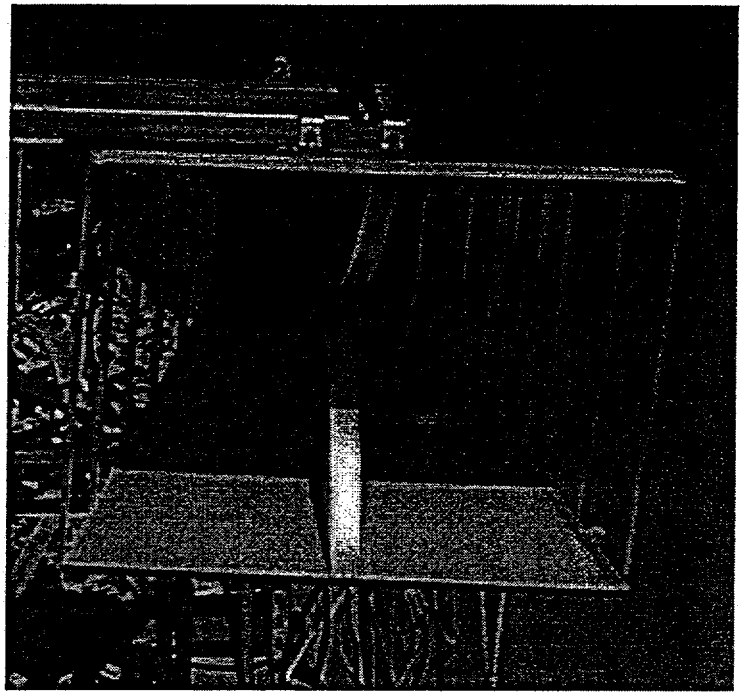

Figure 5. Double-ridged horn transmit antenna

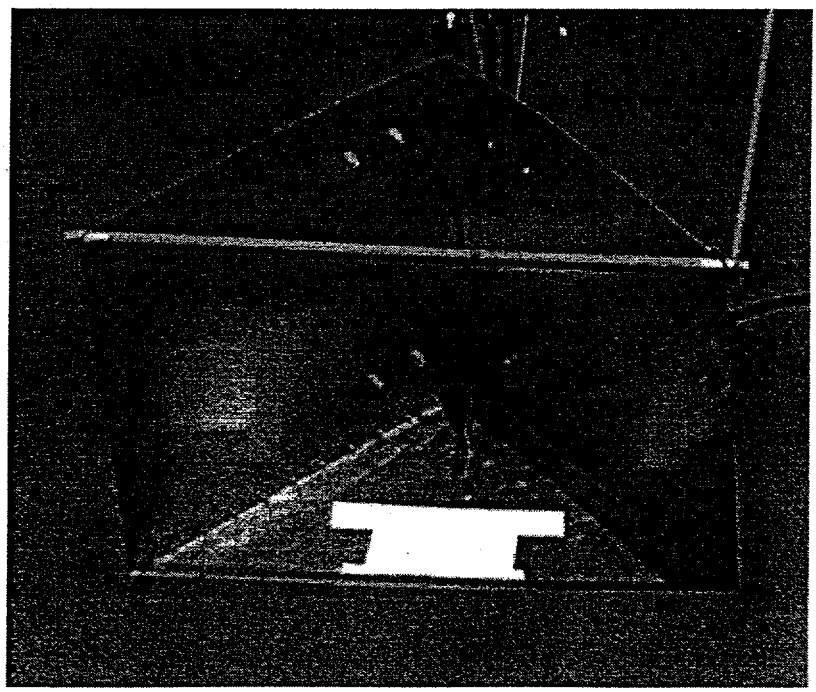

Figure 6. Monopole corner reflector receive antenna

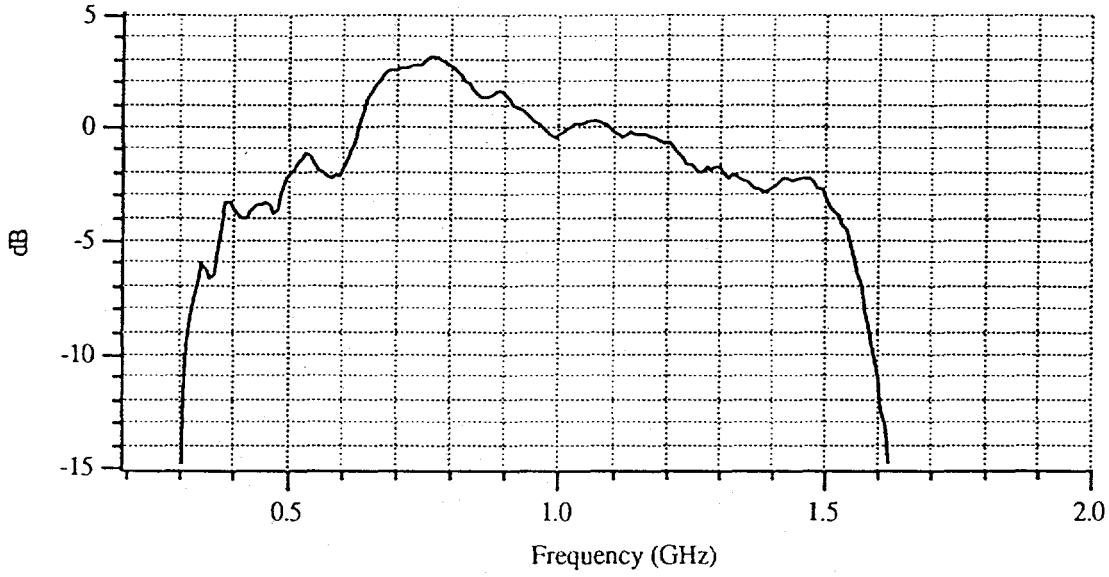

Figure 7. Normalized frequency response of antenna pair

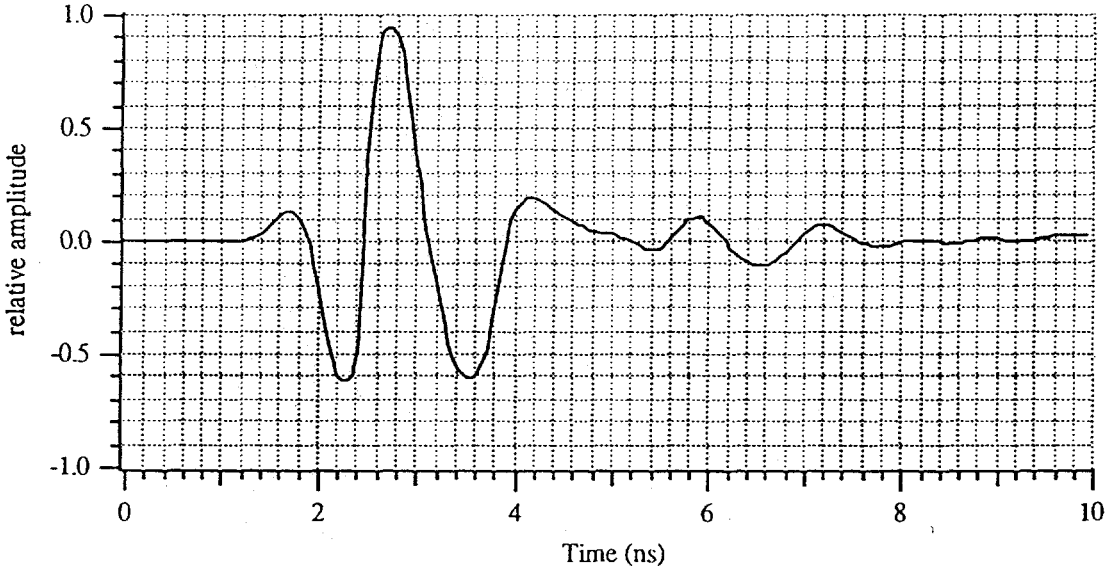

Figure 8. Time-domain response of GPR system

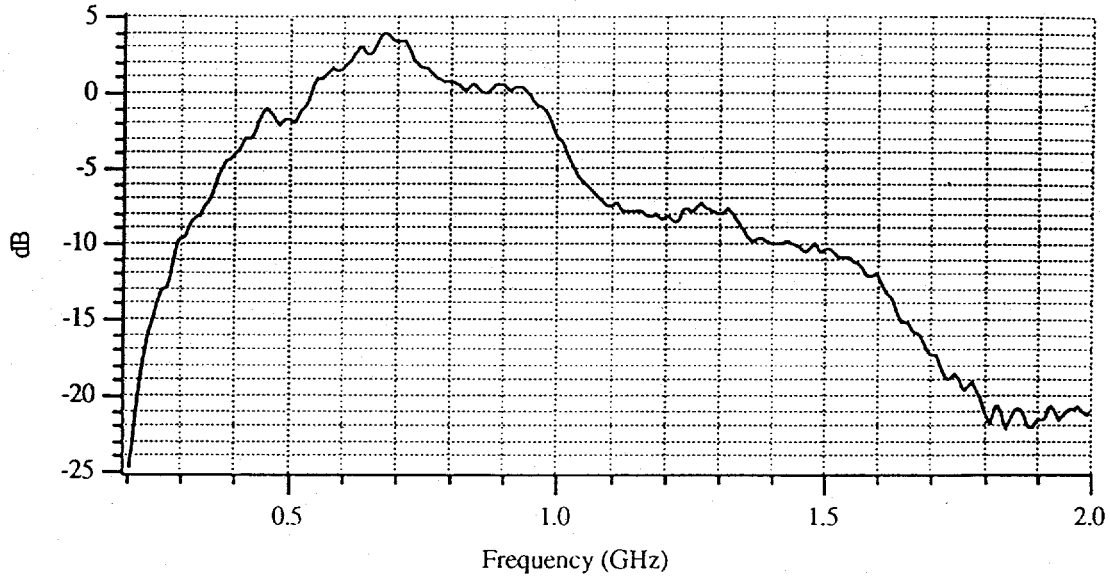

Figure 9. Normalized frequency-domain response of GPR system

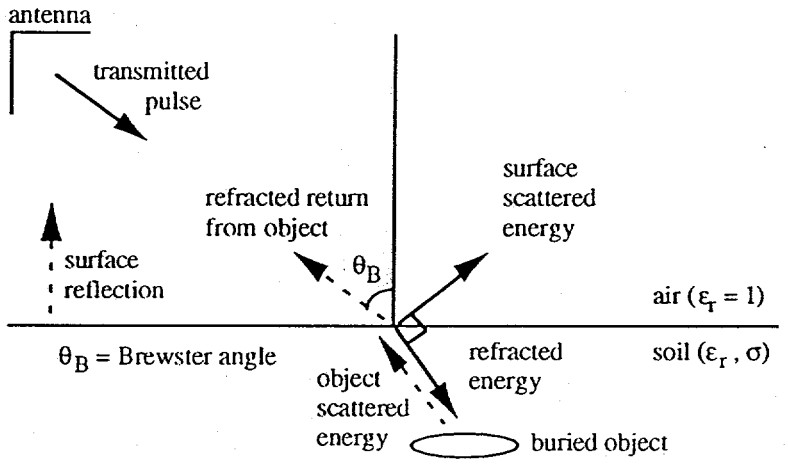

Figure 10. Illustration of rf energy propagation for buried object detection

Figure 11. Buried Object and Mine Detection Facility at the Nevada Test Site

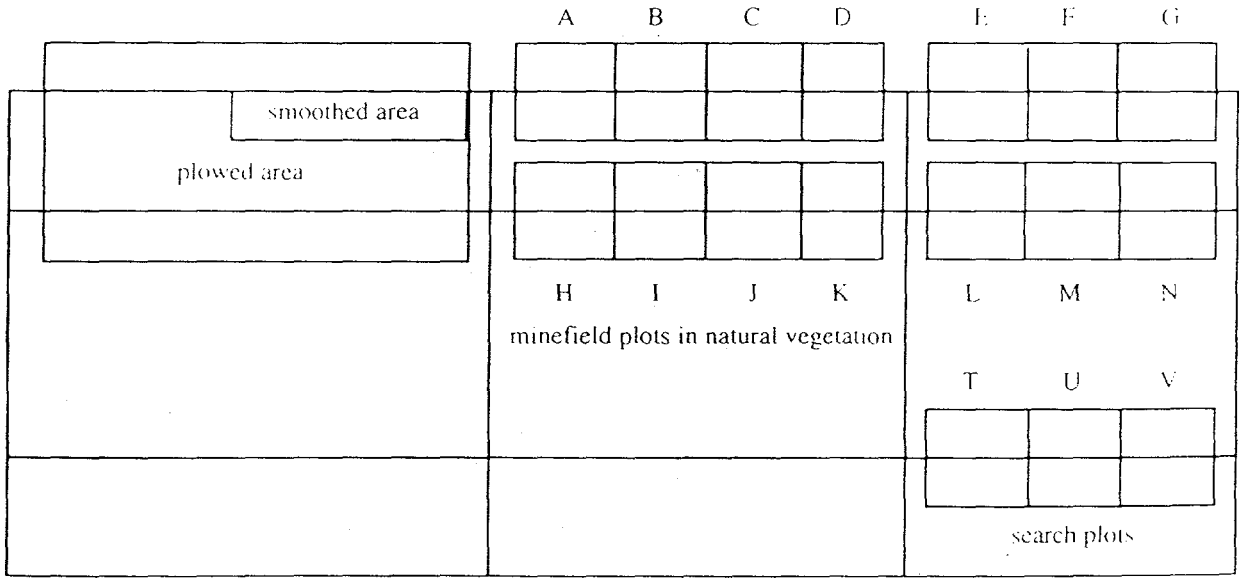

Figure 12. Layout of NTS Mine Detection Facility

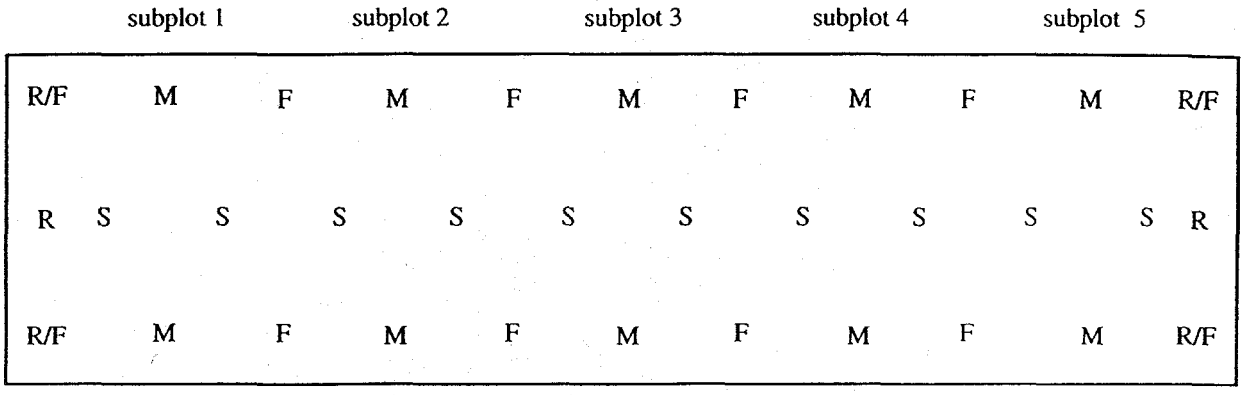

Figure 13. Typical layout of an NTS minefield plot

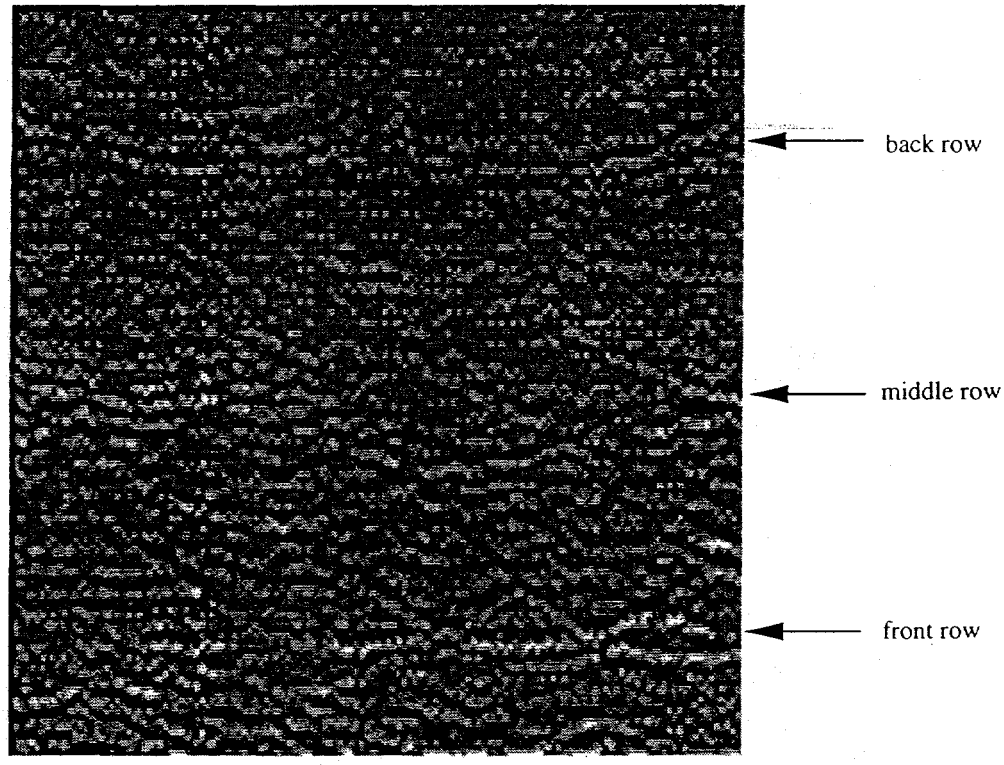

Figure 14. Composite image of minefield IS-4 subplot

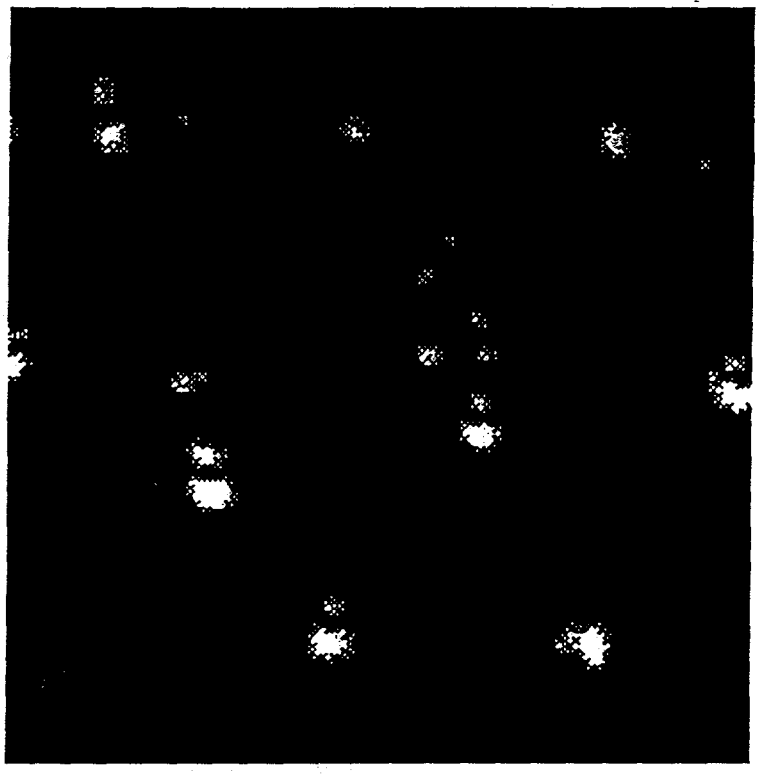

Figure 15. Reconstructed SAR image of minefield subplot IS-4

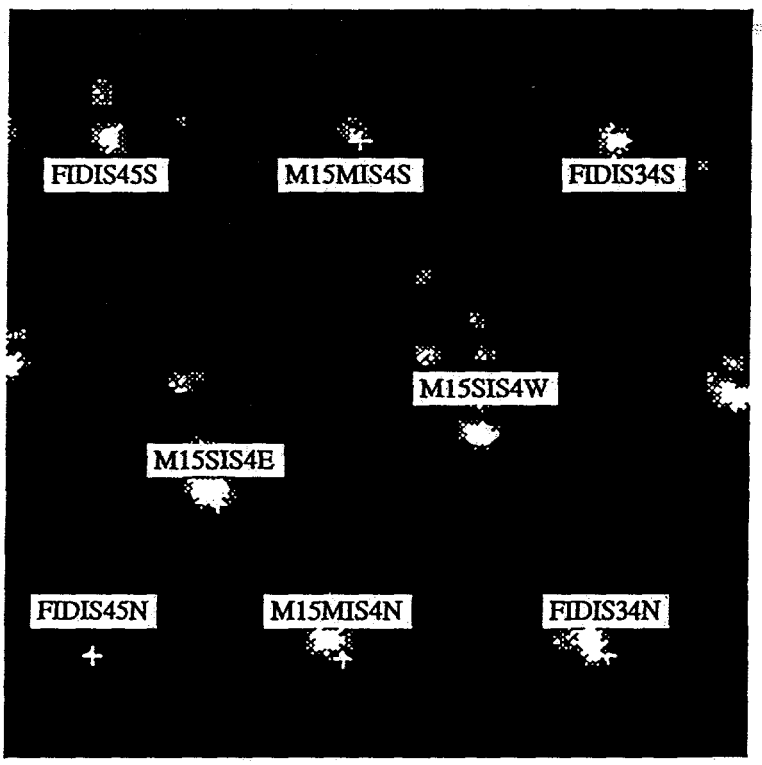

Figure 16. Reconstructed SAR image of IS-4 with ground-truth registration

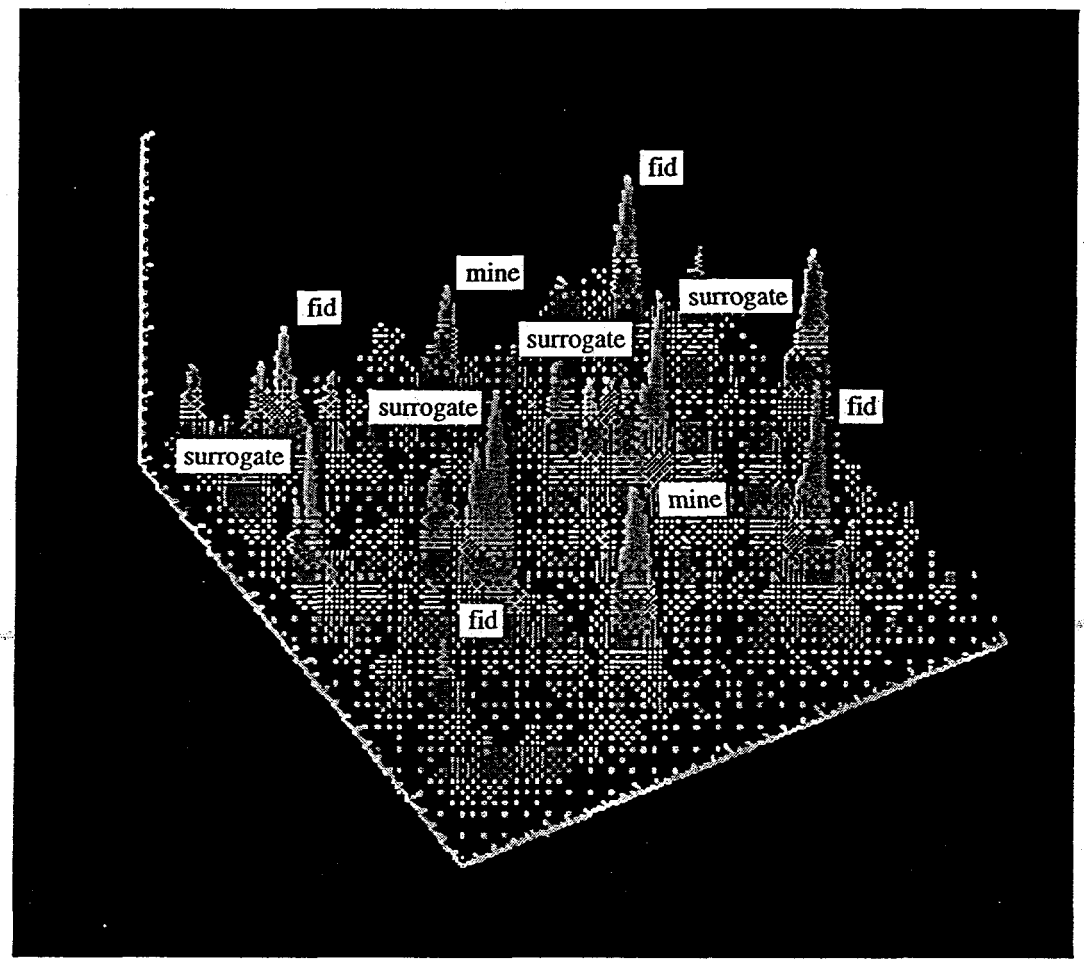

Figure 17. Three-dimensional SAR image of minefield subplot IS-4